



HAL
open science

Roughness characteristic length scales of belt finished surface

Maxence Bigerelle, A. Gautier, B. Hagege, Jérôme Favergeon, B. Bounichane

► **To cite this version:**

Maxence Bigerelle, A. Gautier, B. Hagege, Jérôme Favergeon, B. Bounichane. Roughness characteristic length scales of belt finished surface. *Journal of Materials Processing Technology*, 2009, 209 (20), pp.6103 - 6116. 10.1016/j.jmatprotec.2009.04.013 . hal-01911367

HAL Id: hal-01911367

<https://hal.science/hal-01911367>

Submitted on 13 Apr 2024

HAL is a multi-disciplinary open access archive for the deposit and dissemination of scientific research documents, whether they are published or not. The documents may come from teaching and research institutions in France or abroad, or from public or private research centers.

L'archive ouverte pluridisciplinaire **HAL**, est destinée au dépôt et à la diffusion de documents scientifiques de niveau recherche, publiés ou non, émanant des établissements d'enseignement et de recherche français ou étrangers, des laboratoires publics ou privés.

Roughness characteristic length scales of belt finished surface

M. Bigerelle^{a,*}, A. Gautier^a, B. Hagege^a, J. Favergeon^a, B. Bounichane^{a,b}

^a Laboratoire Roberval, UMR CNRS 6253, UTC Centre de Royallieu, BP 2059 Compiègne, France

^b Equipe Caractérisation et Propriétés des Pêrisurfaces, LMPGM, CNRS UMR 8517, ENSAM, 8, Boulevard Louis XIV, 59046 Lille Cedex, France

ARTICLE INFO

Keywords:

Belt finishing process
Roughness
Finishing
Multi-scale modelling

ABSTRACT

Surface integrity, dynamic properties and mechanical characteristics of belt finished surfaces strongly depend on the achieved surface roughness produced by the abrasion process. A new approach based on the scaling analysis of the roughness characterization is introduced on a surface obtained by a set of roughness process parameters. Experimental results show that range roughness amplitude depends on the scan size and that roughness amplitude follows two stages. Stage I presents a linear power-law roughness distribution—a linear relation. Stage II presents a non-linear power-law roughness distribution. The latter is divided into two sub-stages: the first sub-stage (sub-stage II.a) characterizes the fractal behaviour of the surface until a critical length where the second sub-stage (sub-stage II.b) starts and characterizes roughness by extreme values statistics. Fractal parameters, extreme values estimators and transition scale threshold between stages II.a and II.b are shown to be related to the abrasion process. As a result, an original probabilistic model based on the generalized lambda distribution is proposed to estimate the extreme range amplitude roughness values in stage II, depending on the observation scale. Finally, the maximal roughness amplitude PDF is estimated, at a scale higher than the scanning length with the aid of a bootstrap protocol coupled with a Monte-Carlo simulation.

1. Introduction

Techniques of high precision machining have made important progresses in the last thirty years. Surface topography obtained by high precision machining plays a major role in term of surface functionality. To characterize the surface roughness, a high number of roughness parameters may be used (Whitehouse, 1994; Najjar et al., 2003). One of the most common parameter is the R_a parameter which represents the average roughness amplitude. Although this parameter is highly robust from a statistical point of view, it fails to represent the extreme values of the surface topography. High peaks or deep valleys are not sufficiently characterized by this parameter. However, in a high number of surface functionalities and integrities, the maximal roughness amplitude is of major interest (called R_t , PV or R_z roughness parameter). The transient behaviour of super-finished surfaces has been examined by Malkin and co-workers (Puthanangady and Malkin, 1995; Varghese and Malkin, 1995). They found that the radial stock removal during the transient stage is approximately equal to the average peak-to-valley (PV is another definition of the R_t parameter) surface roughness of the initial ground surface. Chang et al. (2008) have used the R_t parameter to investigate effect of process parameters on evolution of super-finished surfaces texture obtained by stone super-finishing of

hardened AISI 8119 steel. The maximal amplitude is of major interest to characterize the surface defects in the case of optical elements obtained by grinding and lapping processes. All these defects have an effect on the stresses that induce fractures, scratches and micro-cracks that influence operational life, secular stability operational life, secular stability, coating quality and transmission performance (Shen et al., 2005; Fine et al., 2005; Stolz et al., 2005; Retherford et al., 2001; Campbell et al., 2004). Experimental results suggest a linear correlation between SSD (sub surface damage) depth and R_t with a proportionality constant. Values of the proportionality constant have been documented by researchers for various materials: glass (Hed and Edwards, 1987), marble crystal and ruby (Randi et al., 2005), fused silica (Miller et al., 2005). This linear relation was explained and modelled by Miller et al. (2005) by applying micro-indentation mechanics and built models for the SSD/surface roughness ratio based on the indentation of sharp and spherical indenters, with respect to material mechanical properties, shape and load of abrasive grains. However, a new model was created by Li et al. (2008), investigating median and lateral crack systems in brittle surface induced by a sharp indenter, and the contribution of the elastic stress field to the median crack propagation. Finally, subsurface damage depth can be predicted accurately by measuring surface roughness of grinded or lapped optical elements: it exists a non-linear monotone increasing correlation between subsurface damage depth and surface roughness (R_t value). When surface micro-geometry has a significant effect on the local fluctuations in film thickness and pressure, the R_t parameter is important to

* Corresponding author.

E-mail address: maxence.bigerelle@utc.fr (M. Bigerelle).

characterize the mixed regime of micro-elastohydrodynamic and boundary lubrication. These mechanisms are believed to govern most surface failures, such as excessive wear, pitting and scuffing (Spikes and Olver, 2002; Chang, 1995; Cheng, 2002). Krupka et al. (2008) show that changes in the film thickness profiles are more complex in comparison with the case of the isolated artificially produced roughness features (like grooves of various depths, larger or smaller pits and peaks that are located within a concentrated contact). Conversely, peaks disturb the lubricant flow in the contact inlet zone: reduced film thickness area propagates upstream or downstream depending on the slide-to-roll ratio conditions. In the case of electrorheological fluid-assisted polishing, the roughness of the polished surface is characterized by R_t as a function of the applied voltage, the rotational speed of the tool, the rotational speed of the workpiece, a mixing ratio and machining time (Zhanga et al., 2005). In fact, the use of the R_t parameter is justified by a model proposed by Jha and Jain (Jha and Jain, 2006; Das et al., 2008) based on local peaks erosion. This is confirmed by a study made by Yamaguchi and Shinmura (1999): the observed surface texture shows that the process is an accumulation of the micro-scratches from the abrasive cutting edges, generating a characteristic magnetic abrasive finished surface. Moreover, the surface is finished by removing the material from not only the peaks but also the valleys of the surface, as far as the cutting edges of the magnetic abrasive are introduced into the valleys. A same class of peak removal algorithms is also applied on belt finishing process by Bigerelle et al. (2008) and to model abrasive flow machining by Wani and Jain (Wani et al., 2007; Jain et al., 1999). A mathematical model is presented by El-Axira et al. (2008) to predict the R_t parameter caused by internal ball burnishing process parameters (burnishing speed, feed, depth of penetration, and number of passes). Considering the grinding of hard steel to obtain a quality optical surface, Stephenson et al. (2001) show that the presence of voids is responsible of a relatively high R_t . In the particular case of the abrasive finishing, Grzesik et al. (2007) show that the SRz (peak-to-valley height in 3D measurement) and its two components SRp (maximum peak height) and SRv (maximum valley depth) are relevant to characterize surface topography and prove that an elastic belt modifies both valleys and peaks of the surface, whereas a rigid abrasive stone is only able to change the configuration of the peaks.

Another processes of super-finishing require R_t to quantify the surface integrity like lapping (Brinksmeier et al., 2006; Belkhir et al., 2007), surface finishing with flexible abrasive tools (Cho et al., 2002; Singh et al., 2005), finishing milling of complex surface (Ramos et al., 2003), ultrasonic vibration assisted polishing machine (Suzuki et al., 2006), flat end milled surface (Ryua et al., 2006). Some recent studies show that abrasion processes create a multi-scale roughness structure, i.e. the value of roughness will depend on the scale at which it is observed. Bigerelle et al. (2005) show that grinding surface can be modelled by fractal function that is confirmed experimentally on polishing surfaces (Dalla Costa et al., 2007; Giljean et al., 2007, 2008). Wang and Hu (2005) used multi-scale analyses on the inner surface finishing of tubing by magnetic abrasive finishing. They showed that finishing parameters such as polishing speed, magnetic abrasive supply, abrasive material, magnetic abrasive manufacturing process and grain size have critical effects on the material removal rate and the changes of structure of microshape of the surface during finishing. Takaya et al. (2006) analysed the surface finishing of a micropart made of single-crystal silicon and proved that surface roughness gets a spatial wavelength range from 1 μm to 10 nm.

All these studies show that the peak-to-valley parameter is of major interest to characterize the super-finishing process. However, this parameter depends on the evaluation length (Hasegawa et al., 1996; Dubuc et al., 1989) and if we suppose that the scanning area is very small compared to the full area of the part then the R_t param-

eter cannot be evaluated on the whole surface. As a consequence, a multi-scale modelling has to be constructed to extrapolate data from the profile length to the whole sample. In this paper, we propose an original method that allows both predicting maximal range amplitude versus length of the part and giving confidence intervals of the predicted values. It is shown, thanks to a wavelength analyse, that the surface obtained by belt finishing process (BFP) gets a multi-scale structure (Mezghani et al., 2009) and the surface integrity of these tooled surfaces is of major interest to ensure high fatigue performances of the polished surfaces. Axinte et al. (2005) and Novovic et al. (2004) confirmed on a AISI 52100 steel (Rech et al., 2008), where it is shown that the BFP improves very significantly the surface integrity by the induction of strong compressive residual stresses in the external layer and by a great improvement of the surface roughness. This process can be modelled by a peak removal technique (Khellouki et al., 2007) and then it becomes obvious that surface topography of BFP will be well characterized by the R_t roughness parameter (Axinte et al., 2009; Jourani et al., 2005).

For these reasons, we will apply our methodology on the surface topography of a AISI 52100 steel machined by BFP. In a first part, the abrasive process is detailed and the protocol of the roughness measurements is described. After multi-scale analyses of the surface topography obtained by BFP, a prediction model is proposed and validated at different scales. A fractal model is then proposed to confirm the multi-scale aspect of the tooled surface.

2. Grinding belt device

The testing bench is composed of a Bader type grinding belt device set up on a conventional lathe. Consequently, the system has a horizontal structure which is currently used for the grinding belt super-finishing of crankshafts. To be sure of the reproducibility of the process, five bearings are tooled. Their dimensions are 54.78 mm in diameter and 30 mm in width (Fig. 1). The belt is 20 mm width. The tooling movement is composed of a tangential relative part displacement due to its rotation with regard to the belt one and an oscillation of the tooling arm in the axial direction of the tooled part. Specimens were turned, rectified and tooled with the following process:

- Hardness of contact wheel (polyurethane): 90 shores
- Belt grit size: 9 μm
- Contact pressure: 1 bar
- Workpiece rotation speed: 100 rpm
- Belt feed: 50 mm/mn
- Cycle time: 3 s
- Axial oscillation frequency: 1.6 Hz
- Axial oscillation amplitude: ± 0.5 mm
- Lubrication: CUT MAX H05TM

3. Roughness measurements

27 profiles are recorded perpendicularly to the grooves over a 0.1 μm sampling length, a 8 mm scanning length (80,000 amplitude roughness data per profile) and a 100 $\mu\text{m/s}$ scanning speed. The surface recorder is a tactile profilometer 3D KLA TENCOR[®] P10 with a 2 μm stylus radius loaded with 5 mg. The instrument has a vertical resolution better than 10 nm with a lateral x axis resolution of 50 nm and y axis resolution of 1 μm . Each profile was fitted by a least mean square third degree polynomial function to remove the form and keep only waves and roughness. Fig. 2 represents a recorded profile of the tooled surfaces with three spatial zoom (X8, X35, X200) located at the profile origin. As it can be observed, the structure of the surface presents deep valleys and honeys due to the belt finishing process.

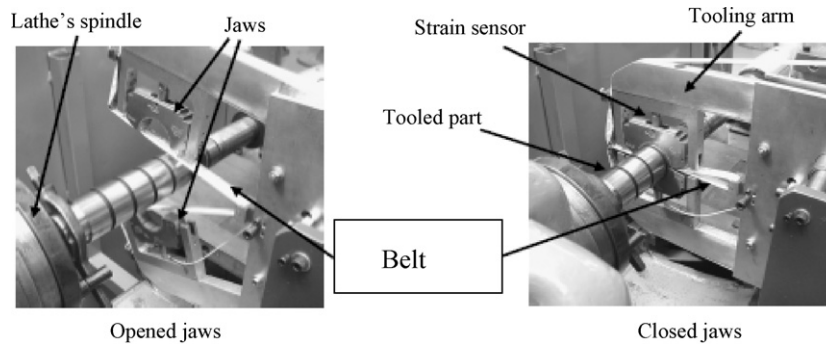


Fig. 1. The grinding belt device.

4. Multi-scale roughness characterization

The arithmetic average roughness parameters (R_a) and the total amplitude one (R_t) also called the “peak-to-valley” are very often used to characterize the surface roughness. Unfortunately, the effect of the evaluation length is not always taken into account although these parameters depend on the observation scale (Dubuc et al., 1989; Whebi, 1986). The dependence of scale measure is defined in the fractal formalism introduced by Mandelbrot (1983) and then was used to characterize the surface roughness (Tricot, 1993).

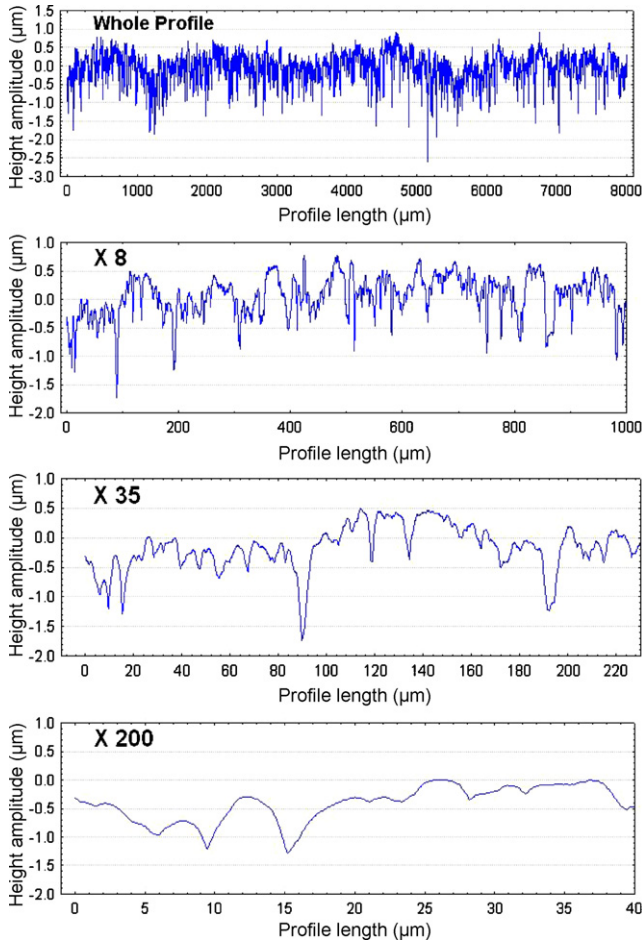


Fig. 2. Recorded profile (whole profile) of the tooled surfaces of AISI 52100 steel machined by belt finishing process with three spatial zoom (X8, X35, X200) located at the profile origin.

4.1. Basic concept

The multi-scale analysis tools are described. The goal of the data management was to compute the roughness amplitude parameter $R_t = Y_{\max} - Y_{\min}$ as a function of the evaluation length. As far as R_t is concerned, it can be expected that the probability to record high peaks (i.e. high value of Y_{\max}) or deep valleys (i.e. small value of Y_{\min}) increases with the evaluation length l . Although the $R_a = \frac{1}{l} \int_0^l |y(x)| dx$ depends on the evaluation length $l \leq l_0$, it becomes constant (result not shown) on the whole profile length L ($L > l_0$) and is equal to $R_a = 0.32 \mu\text{m}$. Other roughness parameters are computed (Table 1). In our algorithm, the values of Y_{\max} and Y_{\min} are computed to calculate a local value of R_t noticed $R_t(x, l) = Y_{\max}(x, l) - Y_{\min}(x, l)$ for a given evaluation length l beginning at the x position of the profile length (x and l varying from 0 to $L = 2$ mm) on the residual profile. Then, the evaluation window of length l is shifted by a quantity d ($d \in [\Delta x, L/2]$) to estimate new local values $Y_{\max}^d(d, l)$, $Y_{\min}^d(d, l)$ and $R_t^d(d, l)$ noted respectively $Y_{\max}^d(l)$, $Y_{\min}^d(l)$ and $R_t^d(l)$. This operation is repeated until the end of the residual profile i is reached giving three sets of local values ($Y_{\max}^d(l)$, $Y_{\max}^{2d}(l)$, $Y_{\max}^{3d}(l)$, ...), ($Y_{\min}^d(l)$, $Y_{\min}^{2d}(l)$, $Y_{\min}^{3d}(l)$, ...), ($R_t^d(l)$, $R_t^{2d}(l)$, $R_t^{3d}(l)$, ...). Then an average is computed on the three sets giving three scalars noted $Y_{\max}(l)$, $Y_{\min}(l)$ and $R_t(l)$ corresponding to an observation scale l for the residual profile.

4.2. Preliminary result

Fig. 3 represents the multi-scale roughness values of $Y_{\max}(l)$, $Y_{\min}(l)$ and at different observation scales l for the 27 recorded profiles. The following primary comments can be declared from these graphics:

- The three roughness parameters $Y_{\max}(l)$, $-Y_{\min}(l)$ and $R_t(l)$ increases logarithmically with the evaluation length l meaning

Table 1

Descriptive statistics of roughness parameters of recorded profile of the tooled surfaces of AISI 52100 steel machined by belt finishing process.

	Mean	Minimum	Maximum	S.D.
R_a	0.32	0.27	0.37	0.03
R_q	0.40	0.36	0.53	0.05
Sk	-1.4	-2.1	-0.8	0.3
Ek	8.2	4.5	14.1	2.3
R_t	4.8	3.0	7.0	1.0
Lac	12.6	10.1	15.5	1.6
Peaks	1315	1205	1475	69
Sm	19.2	17.1	20.9	0.9
Rpk	0.6	0.3	1.5	0.3
Rk	0.9	0.7	1.0	0.08
Rvk	3.3	1.6	5.4	0.9
Fractal dimension	1.141	1.129	1.151	0.006

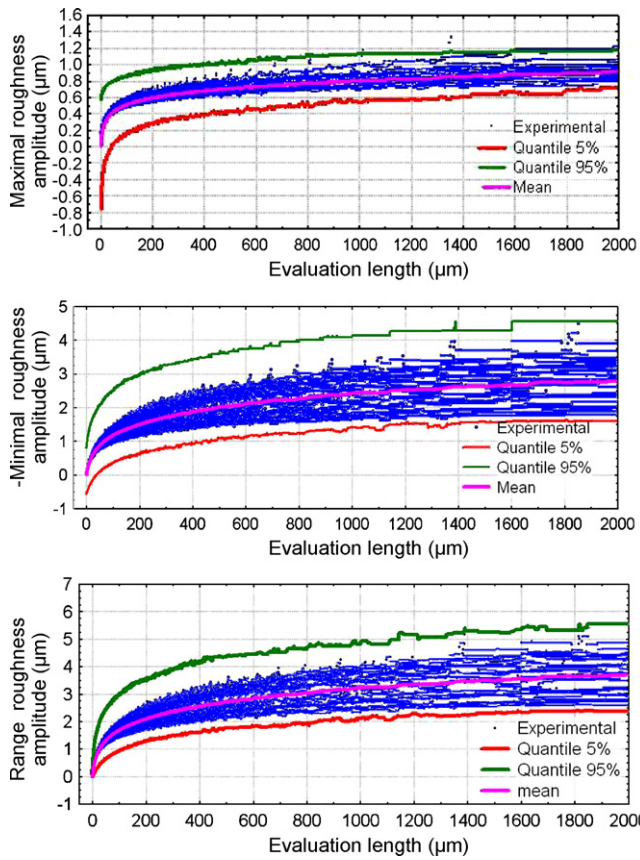


Fig. 3. Multi-scale roughness values of $Y_{\max}(l)$, $Y_{\min}(l)$ and $R_r(l)$ versus the evaluation scales l for 27 recorded profiles of AISI 52100 steel with belt finishing process.

that amplitude of peaks and valleys decreases with the scale (see Fig. 2).

- $-Y_{\min}(l) \gg Y_{\max}(l)$ whatever the value of the evaluation length (see Fig. 4). For example $Y_{\max}(2 \mu\text{m}) = 0.086 \mu\text{m}$ increases to $Y_{\max}(2000 \mu\text{m}) = 0.1 \mu\text{m}$ and $-Y_{\min}(2 \mu\text{m}) = 0.91 \mu\text{m}$ increases to $-Y_{\min}(2000 \mu\text{m}) = 2.77 \mu\text{m}$. This roughness signature was not met in the case of micro-machined surfaces (Bigerelle et al., 2008). This multi-scale difference characterizes the BFP that can be seen as peak removal process that decreases more the peaks amplitude than the valleys amplitude as discussed in the intro-

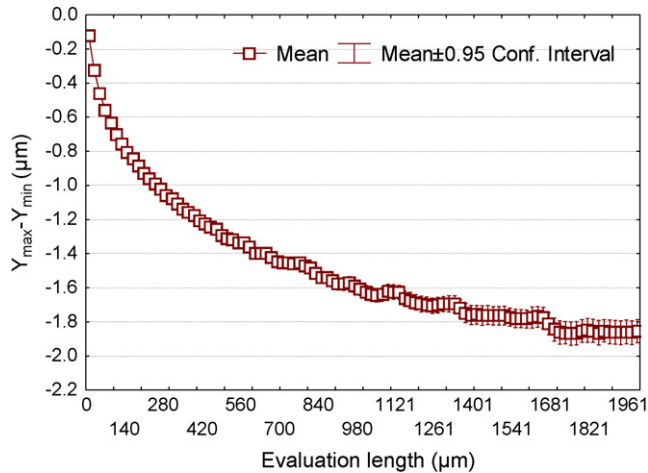


Fig. 4. Multi-scale mean roughness values of $Y_{\max}(l) - Y_{\min}(l)$ at different evaluation scales l obtained by averaging the $Y_{\max}(l) - Y_{\min}(l)$ on the 27 recorded profiles as shown in Fig. 1.

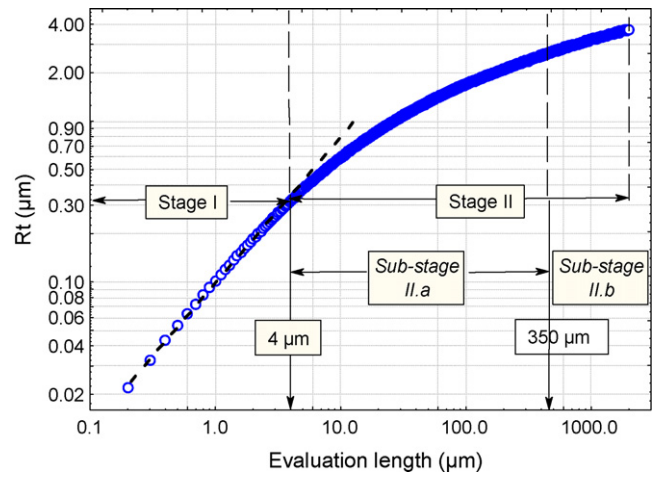


Fig. 5. Multi-scale mean roughness values of $R_r(l)$ at different evaluation scales l obtained by averaging $R_r(l)$ on the 27 recorded profiles as shown in Fig. 1.

duction. An original result given by this analysis is that the difference $Y_{\max}(l) - Y_{\min}(l)$ is always negative whatever the evaluation length l meaning that local small peaks are also removed and not limited to the higher global peaks. Thanks to this multi-scale analysis, this relationship can be explained by the fact that the contact area between abrasive grains and part is small due to the circular shape of the contact wheel leading to local peaks erosion in this contact area.

- Dispersion of the roughness parameters estimations increases with the evaluation length l . As it can be observed, curves are more and more scattered as the evaluation length increases. This second scale effect constitutes the basic concept of this paper and will be discussed later. However, it clearly means that the accuracy to predict a maximal or minimal values depends drastically of the evaluation length and will be less and less precise as the evaluation length increases.

4.3. The different stages of the multi-scale analysis

For each experimental profile under consideration, the averaged local values $R_r(l)$ of the 27 related residual profiles are all averaged to obtain a final R_r value at an evaluation length l . Fig. 5 shows the variation of $R_r(l)$ versus the evaluation length in log-log coordinates. From this graphics, it can be observed that two different stages emerge: a linear stage and a logarithmic one. With appropriate statistical techniques developed earlier to describe the different stages in fatigue crack growth propagation (Bigerelle and Lost, 1999), it can be stated that these two stages limits are:

- Stage 1: $l \leq 4 \mu\text{m}$ (log-log linear stage),
- Stage 2: $l > 4 \mu\text{m}$ (log-log logarithmic stage).

Here, this analysis is purely visual. Basically as met in the bibliography, one could think that we are in presence of a bi-fractal structure (Wu, 2000; He and Zhu, 1997; Thomas et al., 1999; Bhushan and Majumdar, 1992; Wu, 2001). The linear part represents the fractal part (stage 1) and the second one, a pseudo asymptotical stage. In our case, this bifractal structure does not hold. We will prove that in fact the linear part is a measure artifact due to the stylus radius of the profilometer and that the second stage is composed of two sub-stages: a non-linear fractal stage (sub-stage II.a) and an “extreme values stage” (sub-stage II.b). For reason of simplicity, we voluntary introduce first the fractal stage to analyse these three stages.

4.4. Stage II.a: the fractal stage

The fractal concept with the R_t value was introduced by Dubuc et al. (1989) that has developed a method to calculate the fractal dimension of profiles called “the oscillation method”. This method introduces the τ -oscillation of the function f in x defined as

$$f : [a, b] \rightarrow \mathbb{R}$$

$$OSC_\tau(f, x) = \left| \frac{\max_{|x-t|<\tau}(f(t)) - \min_{|x-t|<\tau}(f(t))}{\tau} \right| \quad (1)$$

by taking the average of $OSC_\tau(f, x)$ within the interval $[a, b]$, one obtains:

$$VAR_\tau(f, a, b) = \frac{1}{b-a} \int_a^b OSC_\tau(f, x) dx \quad (2)$$

So that the fractal dimension is written as

$$\Delta(f, a, b) = \lim_{\tau \rightarrow 0} \left(2 - \frac{\log VAR_\tau(f, a, b)}{\log \tau} \right) \quad (3)$$

By roughness analogy one has:

$$R_t^\alpha(l) = OSC_l(f, x) \quad (4)$$

where function f is given by our experimental profile f_e and under this consideration, from Eq. (2):

$$R_t(l) = VAR_l(f, 0, l) \quad (5)$$

From Eq. (3), the fractal dimension $\Delta(f_e, 0, l)$ of the f_e profile is equal to 2 minus the slope called the Hölder exponent.

However, except in the stage I, no linear relation is found (Fig. 5). It must be also noticed that in a large number of papers, a perfect linear stage is never met. Why does the linearity not perfectly hold? We search if this non-linearity could not be due to a sampling problem. By analyzing Fig. 5, it become obvious that above the value of $4 \mu\text{m}$, the R_t values less and less increase with respect to the profile length, meaning that if the fractal concept holds (i.e. linearity in the log-log scale), the R_t values are less and less underestimate as the evaluation length increases. An explanation of this bias can be stated: the number of data points is imposed by the profilometer (80,000 in this study) meaning that for small evaluation lengths, the R_t value is computed with a finite number of points and this number increases with the evaluation length. If one gets an infinity of points to evaluate the R_t value then the R_t estimation will converge to the true value of the R_t parameter. Unfortunately, as the number of points is limited, the probability to obtain the true maximal range amplitude on a fixed interval length diminishes with the number of points. This leads that the R_t value will be more and more underestimate when the evaluation length diminishes. To validate this hypothesis, a simulation will be proposed. A perfect Brownian profile ($\Delta = 1.5$) will be simulated by an algorithm process (Spitzer, 1976) (Fig. 6). This choice is justified by the fact that no artifact is introduced by this simulation to the opposite of simulations with partial Brownian motion (Zhou and Lam, 2005). The implanted algorithm consists of 6 steps:

- Step 1: a Brownian motion is simulated with a high number of points (5×10^5).
- Step 2: a windows size l is chosen.
- Step 3: a set of k uniformly distributed points are taken into this windows to estimate the R_t noted $Rt_k(l)$.
- Step 4: another k value is taken and step 3 is repeated.
- Step 5: another length of windows size is taken and step 2 to step 4 is repeated.
- Step 6: goto step 1 to average values of $Rt_k(l)$.

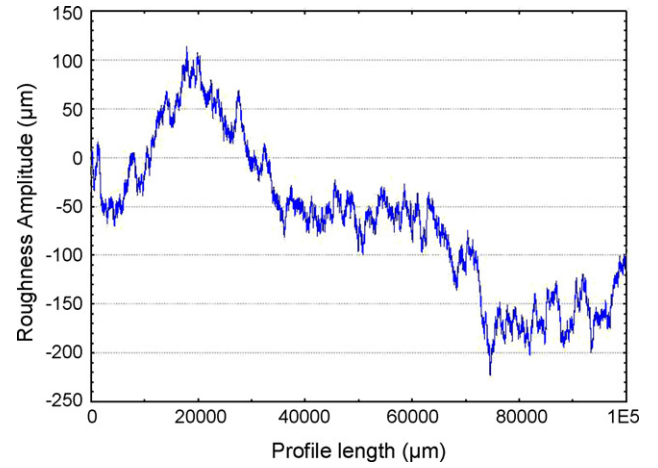


Fig. 6. Simulated profile corresponding to a trace of a perfect Brownian motion.

Fig. 7 represents the values of $Rt_k(l)$ versus the number of points k used to estimate R_t for different window sizes (l). For a given interval length, the R_t values increase with the number of points but this increase is less and less significant. This clearly confirms our basic hypothesis: R_t values are more and more underestimated as the number of points used to estimated R_t decreases. As the windows size l decreases, the R_t values also decreases because of the fractal aspect of Brownian motion. This sampling effect introduces an artifact leading to a non-linear stage. To represent this artifact, R_t values are plotted (in log-log scale) versus the evaluation length with a fixed number of points used to estimate the R_t value for all the evaluation length (Fig. 8). Two remarks have to be made:

- If the number of points is constant to estimate the R_t value for all evaluation length then a perfect linear relation hold.
- The intercept decreases with the number of points used to estimate the R_t value.

To conclude, R_t is uniformly underestimated (in log-log coordinates) as the number of points used to estimate the R_t decreases but the linear part stay unchanged (in log-log scale). More drastic, if the number of points used to estimate R_t increases proportionally with respect to the evaluation length, the slope will be higher than the true value (Hölder exponent) leading to diminish the computed fractal dimension. To visualize this artifact, fractal dimension

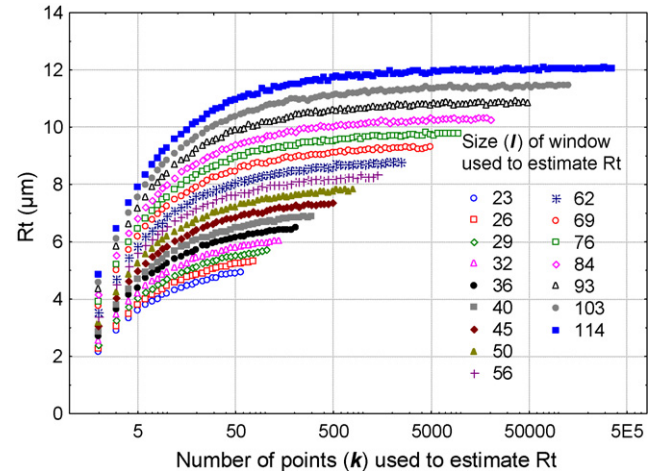


Fig. 7. Values of $Rt_k(l)$ versus the number of points k used to estimate R_t for different window sizes (l) corresponding to the profile shown in Fig. 6.

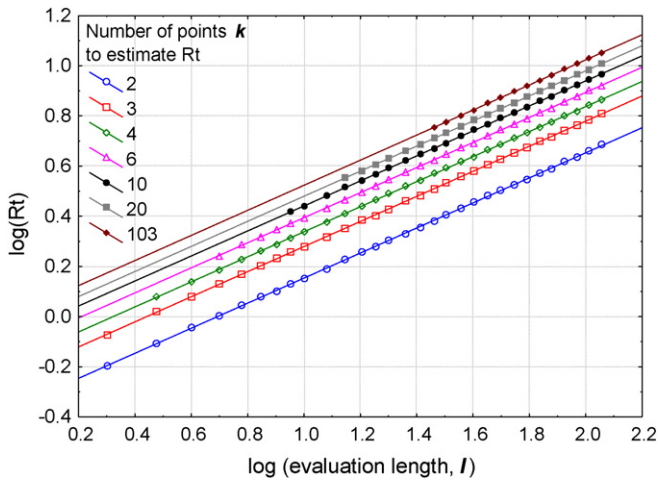


Fig. 8. Values of $Rt_k(l)$ evaluated on a perfect Brownian motion (Fig. 6) versus the evaluation length when $Rt_k(l)$ is evaluated with k points on all window of sizes (l) corresponding to the profile shown in Fig. 6.

is computed versus the number of points used to estimate R_r . More than 10^8 points are required to obtain an error less than 1% (Fig. 9a). If the number of point stays unchanged on all windows whatever their lengths, no error occurs on the evaluation of the fractal dimension, and thus whatever the maximal windows size and the total number of points of the discretized profile (Fig. 9b). To the knowl-

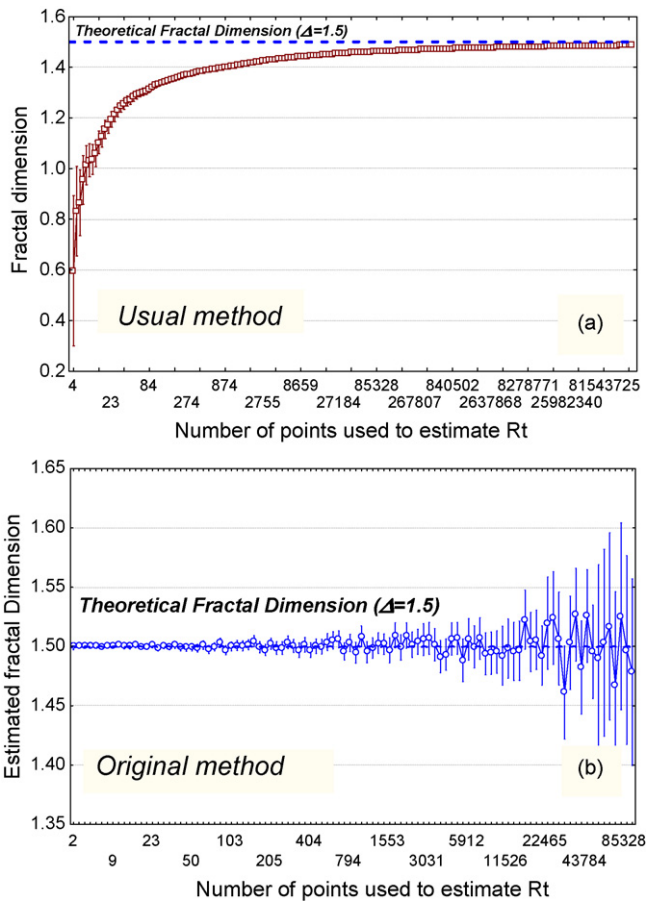


Fig. 9. Values of fractal dimension of a perfect Brownian motion of theoretical value of 1.5 calculated by the Oscillation method (Eq. (3)) when $Rt_k(l)$ is evaluated on with different k points on all window of sizes (l) with $l = p \times k$, p a scale independent constant (usual method (a)) and with a constant number of points for all windows of size l (original method (b)).

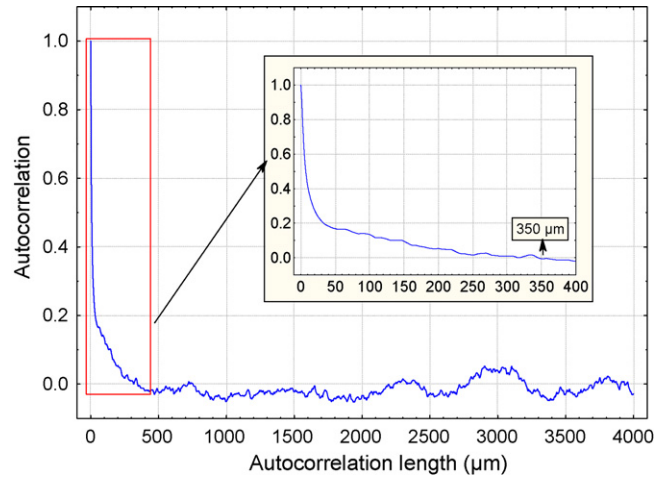


Fig. 10. Average autocorrelation functions of the 27 recorded profiles for 27 recorded profiles of AISI 52100 steel with belt finishing process.

edge of the authors, this statistical artifact was never commented in the bibliography and this statistical bias leads some authors to oversample signals to diminish this artifact effect and then estimate more precisely the fractal dimension by diminishing the bias amplitude. A new algorithm of computation of the fractal dimension, without sampling artifact, applied on real experimental profile may emerge from these results and authors work on this: results will be deferred in another paper (Fig. 10).

4.5. Stage I: the stylus radius tip stage

Profiles appear smoother when $l < 4 \mu\text{m}$ and this value l is exactly the diameter of the tip of the profilometer. The stylus curvature radius makes a smoothing effect of the surface. The stylus cannot record any information into crevices which are narrower than the stylus width (Poon and Bhusham, 1995; Mc Cool, 1986; Radhakrishnan, 1970; Whitehouse, 1974; Nakamura, 1966; Ohlsson et al., 2001; Sheiko et al., 1994; Mazeran et al., 2005). To analyse the stylus effect on surface integration, an algorithm is developed to simulate the stylus effect on profile. However, our recorded surfaces present the stylus effect and as a consequence surfaces without stylus integration effect have to be re-created. To create these surfaces, a model that simulates the BFP effect on surface topography (Bigerelle et al., 2008) is used. This model is based on fractal function that represents initial profile before belt finishing processing (Fig. 11) and two “wear” parameters that characterize wear intensity and material hardness. Fig. 12 represents surface simulated after belt finishing processing corresponding to the experimental profiles used in this study. An algorithm simulating the scan-

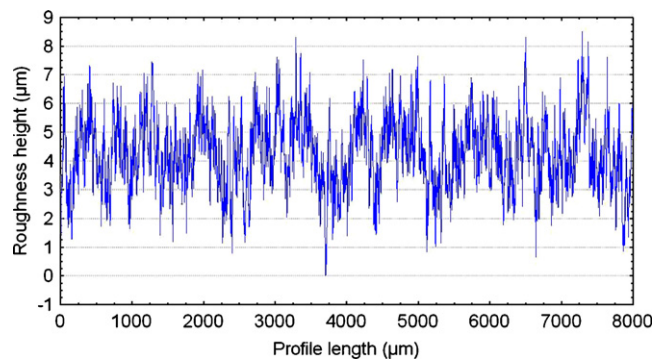


Fig. 11. Fractal modelling of initial grinded surfaces before applied belt finishing surface.

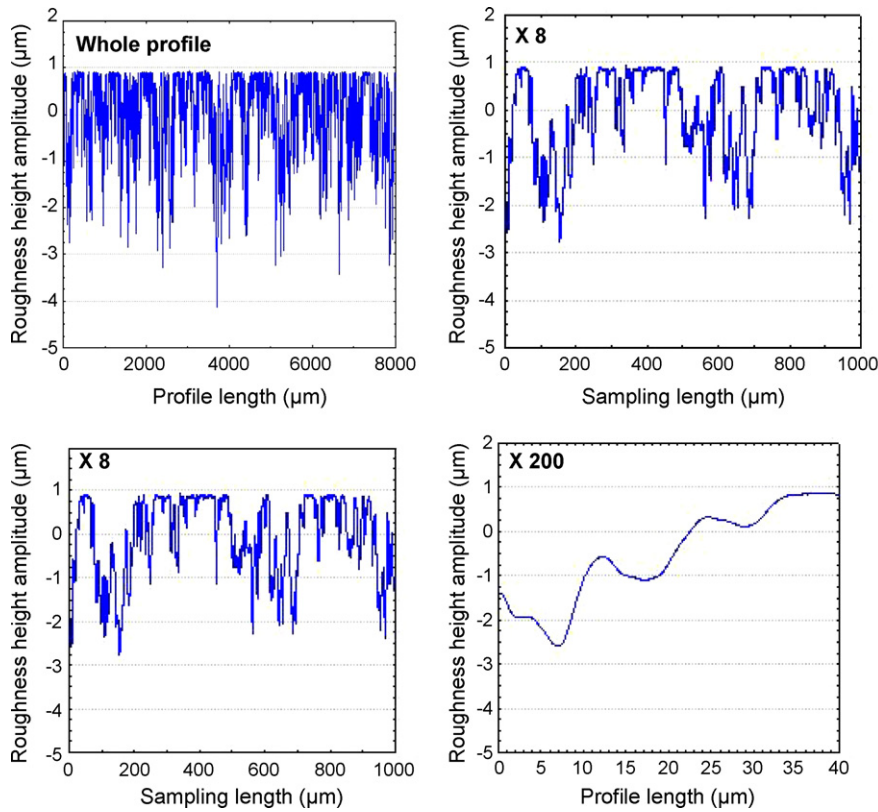


Fig. 12. Simulated profile (whole profile) of the tooled surfaces of AISI 52100 steel machined by belt finishing process with three spatial zoom (X8, X35, X200) located at the profile origin simulated by Bigerelle et al.' model (Bigerelle et al., 2008) without low frequency wave forms with stylus integration of $r = 2 \mu\text{m}$.

ning effect on the profile is written without using mathematical assumption because of the non-derivability of fractal curves. Stylus scanning effect was simulated with radii curvatures from $1 \mu\text{m}$ to $5 \mu\text{m}$. From Fig. 13 the threshold Stage I and Stage II, appear around $4 \mu\text{m}$ for a tip diameter of $4 \mu\text{m}$ and increases with the stylus tip radius. This simulation confirms the fact that this linear stage is due to the effect of smoothing surfaces caused by the tactile covering.

As it is observed, modelling the BFP is very relevant to model high finished surfaces at all scales because multi-scale measures of R_t on experimental (Fig. 5) and simulated surfaces (Fig. 17) are quite similar, and thus, whatever the scales of observation.

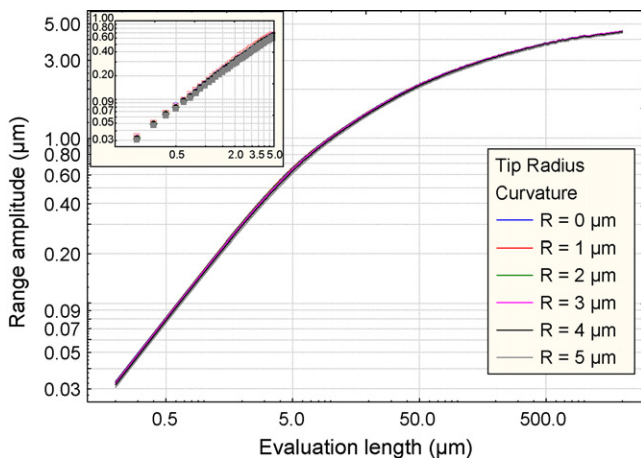


Fig. 13. Multi-scale roughness values of $R_t(l)$ at different observation scales l computed from simulated profile with stylus integration processed at different radii.

5. The macroscopic multi-scale analysis of the amplitude roughness

As shown, a fractal stage can be non-linear due to sampling problems. However, it becomes obvious that the fractal formalism on tooled surface cannot be applied for high evaluation length. Intuitively, we may admit that above a critical length, the fractal concept fails, meaning that physical processes that create the fractal aspect do not affect the surface morphology. In mathematical terms, above this critical length, profiles have lost the memory of the topography. This loss of memory can be quantified by the autocorrelation function. It is reported in the bibliography that autocorrelation function can be used to determine fractal properties of profiles (Lopez et al., 1994; Mandelbrot and Van Ness, 1968). The average autocorrelation function of all profiles is plotted in Fig. 10. As it can be observed, the autocorrelation decreases until it reaches a null value (in average) for $l > 350 \mu\text{m}$. After the stage II, no "memory" occurs in the profile that becomes a pure random process and must be analysed with appropriate tools. This Stage II.b but more especially the length value of the threshold Stage II.a and Stage II.b is of major interest in finishing processes because it quantifies the scale above which the process parameters will not influence the topography and any modification of the process that can decrease the R_t value. This result is fundamental in the dimensional tolerance of tooled parts. To check the assertion that above the fractal stage, the increase of the maximal roughness amplitude is due only to a pure random process (independent of the processing conditions), a mathematical formalism is described in the next paragraph.

5.1. A new stage: the extreme values stage (sub-stage II.b)

Does the recorded signal exhibits a pure stochastic process above $l > 350 \mu\text{m}$? In fact, a new concept was introduced and applied

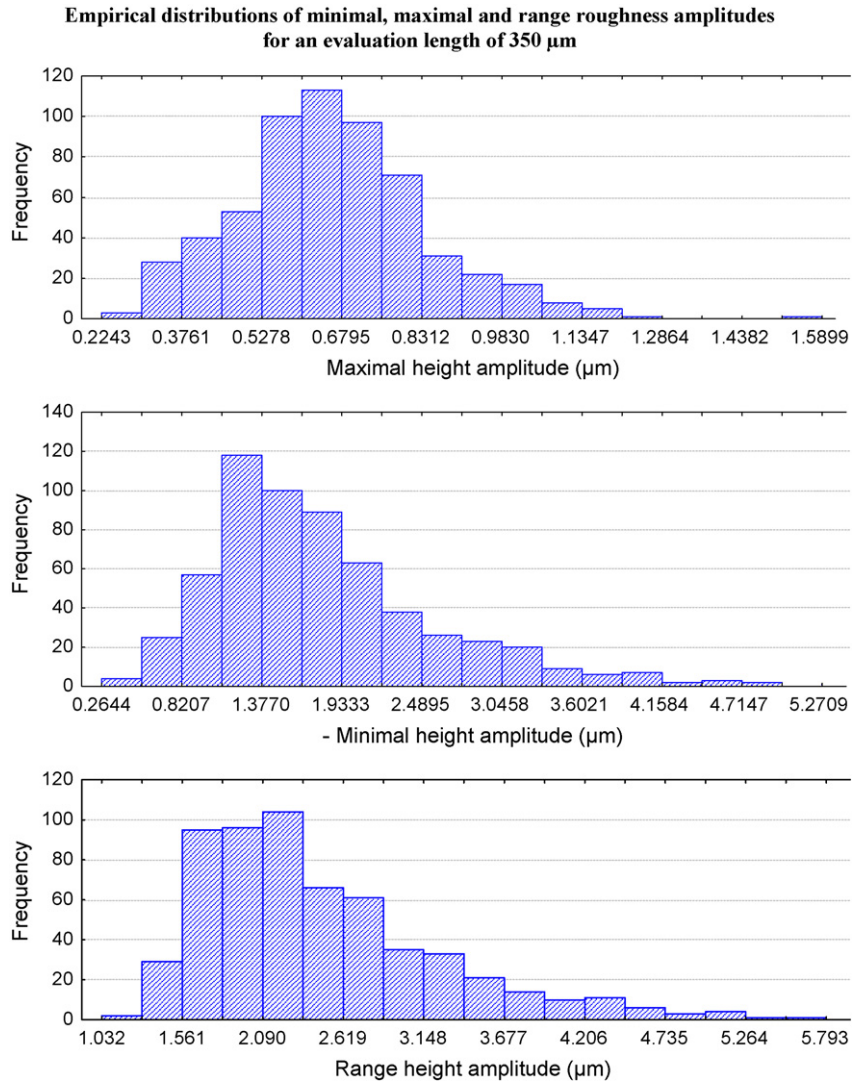


Fig. 14. Empirical distributions of: minimal $Y_{\min}(l)$, maximal $Y_{\max}(l)$, and range roughness amplitude $R_t(l)$ at the evaluation scale $l=350 \mu\text{m}$.

accurately on milling surfaces tooled by single diamond turning (Bigerelle et al., 2007). Above the fractal stage, the surface becomes stationary in a statistical sense (ergodicity) meaning that the mean amplitude of the surface stays constant but the mean is calculated in term of mathematical integration without including sampling effect as described previously in stage II.a. However, including sampling effect, the fluctuation occurs due to inherent stochastic process and the magnitude of the extreme values increases with the number of sampling points. The most successful method of safety or reliability was found in the application of the statistical extreme-value analysis using the Gumbel distribution (Gumbel, 1954) to predict the maximum value of pits on a surface. Because of some limitations (i.e. no confidence intervals for extreme value predictions, properties of the parent distribution are imposed), an alternative methodology to the Gumbel distribution is proposed.

5.2. Extreme amplitude roughness modelling

The surface roughness parameters $Y_{\max}(l)$ and $Y_{\min}(l)$ are measured at a given observation scale l and it raises the following issue: “what will be the values of these parameters at a higher scale that was not measured and what will be the error in the prediction?” The answer to this question is of major interest for the control of high finished surfaces because surface roughness

is seldom measured on the whole part (high time consuming, limitation of scanning length of profilometers, etc.). To predict roughness amplitude at higher scales, we suppose that the evaluation length is above the fractal stage ($l > 350 \mu\text{m}$) and then the Stage II.b has to be modelled. Our methodology is based on the generalized lambda distribution formalism (GLD) (Karian and Dudewicz, 2000) and the use of a Monte-Carlo method. The histograms of all sets $(Y_{\max}^d(350 \mu\text{m}), Y_{\max}^{2d}(350 \mu\text{m}), \dots), (Y_{\min}^d(350 \mu\text{m}), Y_{\min}^{2d}(350 \mu\text{m}), \dots), (R_t^d(350 \mu\text{m}), R_t^{2d}(350 \mu\text{m}), \dots)$ are presented in Fig. 14. The first phase consists in modelling these histograms thanks to the use of the lambda distribution. The generalized lambda distribution (GLD) family is specified in terms of its percentile function (called also the inverse distribution function) with four parameters ($\lambda_1, \lambda_2, \lambda_3$ and λ_4):

$$Q_X(y; \lambda_1, \lambda_2, \lambda_3, \lambda_4) = \lambda_1 + (y^{\lambda_3} - (1-y)^{\lambda_4})/\lambda_2 \quad (6)$$

The parameters λ_1 and λ_2 are, respectively, the location and scale parameters, while λ_3 and λ_4 determine respectively the skewness and the kurtosis of the GLD. The probability density function $f_X(x)$ can then be easily expressed from the percentile function of the GLD:

$$f_X(x) = \frac{\lambda_2}{(\lambda_3 y^{\lambda_3-1} + \lambda_4 (1-y)^{\lambda_4-1})} \quad (7)$$

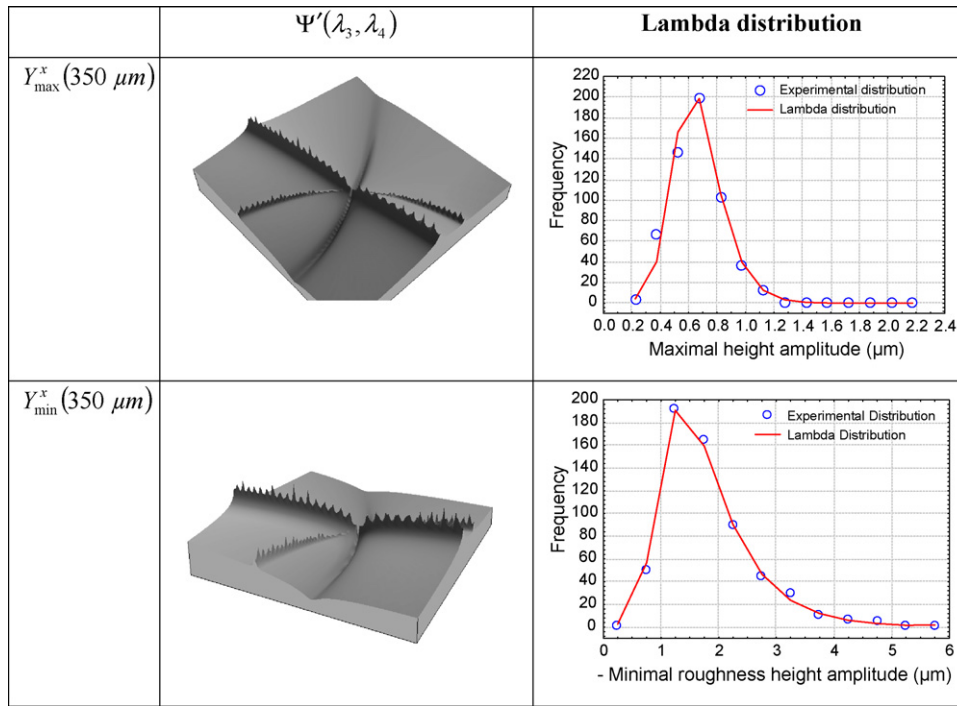


Fig. 15. 3D view of the values of the function $\Psi(\lambda_3, \lambda_4)$ for the lambda distribution associated with $Y_{\max}^x(350 \mu\text{m})$ and $Y_{\min}^x(350 \mu\text{m})$. On the right, $Y_{\max}^x(350 \mu\text{m})$ and $-Y_{\min}^x(350 \mu\text{m})$ lambda distribution obtained after minimization on $\Psi(\lambda_3, \lambda_4)$.

Obviously, the main problem is to estimate the parameters λ_1 , λ_2 , λ_3 and λ_4 in order to have the best fitting of the GLD with the experimental frequency distribution (of extreme roughness values in this study). In a first step, empirical moments are calculated from n experimental data $x_i, i \in \{1, 2, \dots, n\}$:

$$\hat{\alpha}_1 = \sum_{i=1}^n \frac{x_i}{n} \quad (8)$$

$$\hat{\alpha}_2 = \sum_{i=1}^n \frac{(x_i - \hat{\alpha}_1)^2}{n} \quad (9)$$

$$\hat{\alpha}_3 = \sum_{i=1}^n \frac{(x_i - \hat{\alpha}_1)^3}{n\hat{\alpha}_2^{3/2}} \quad (10)$$

$$\hat{\alpha}_4 = \sum_{i=1}^n \frac{(x_i - \hat{\alpha}_1)^4}{n\hat{\alpha}_2^2} \quad (11)$$

Table 2
Moments of $Y_{\max}^x(350 \mu\text{m})$ and $Y_{\min}^x(350 \mu\text{m})$ distributions.

	$\hat{\alpha}_1$	$\hat{\alpha}_2$	$\hat{\alpha}_3$	$\hat{\alpha}_4$
$Y_{\max}^x(350 \mu\text{m})$	0.663	0.193	1.492	10.69
$Y_{\min}^x(350 \mu\text{m})$	1.791	0.790	1.423	5.797

Table 3
Values of the four parameters for the both lambda distributions that modelled $Y_{\max}^x(350 \mu\text{m})$ and $Y_{\min}^x(350 \mu\text{m})$.

	λ_1	λ_2	λ_3	λ_4
$Y_{\max}^x(350 \mu\text{m})$	0.596	1.085	-0.123	-0.0632
$Y_{\min}^x(350 \mu\text{m})$	1.091	0.0754	0.0060	0.0625

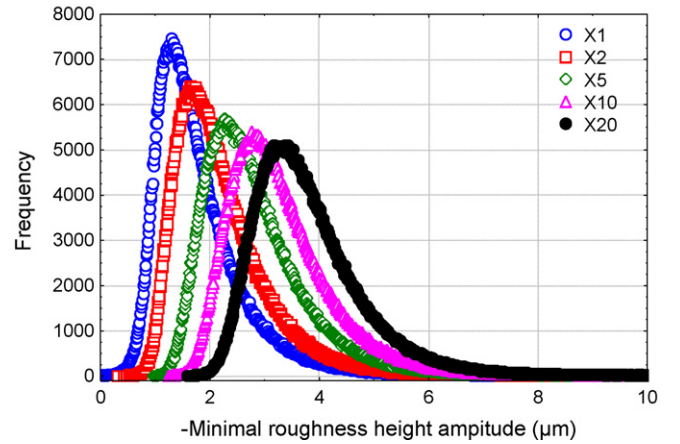
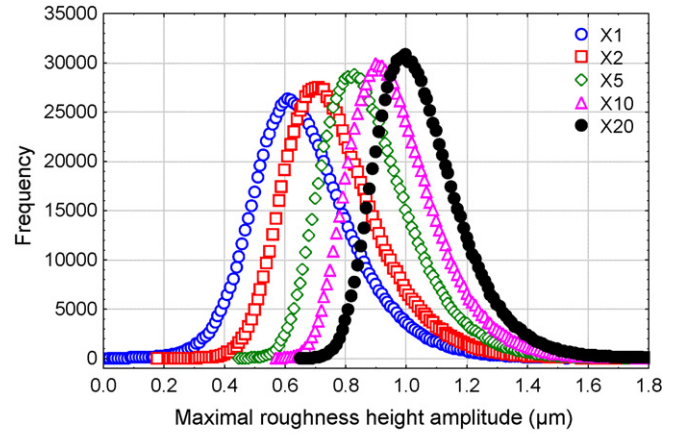


Fig. 16. $\hat{Y}_{\max}^{350 \mu\text{m}, k}$ and $-\hat{Y}_{\min}^{350 \mu\text{m}, k}$ PDF's functions prediction obtained from 100,000 Monte-Carlo simulation for the 5 magnifications $k \in \{1, 2, 5, 10, 20\}$. The case $k=1$ corresponds to simulation of the original lambda shown in Fig. 15 (on the right).

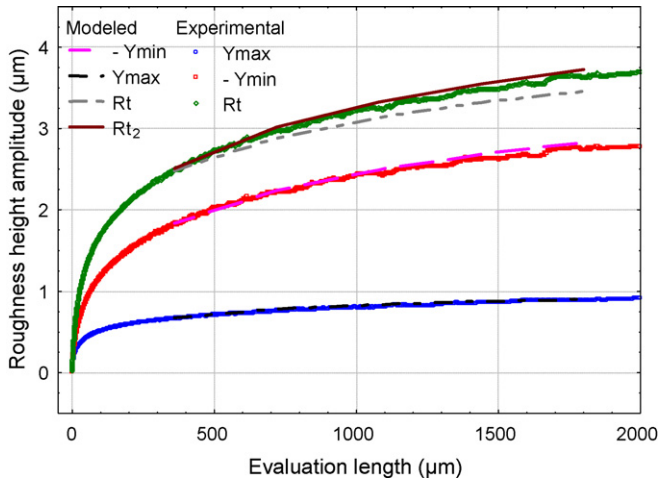


Fig. 17. Prevision of the mean of the extreme roughness amplitude parameters $-\hat{Y}_{\min}^{350\mu\text{m},k}$, $\hat{Y}_{\max}^{350\mu\text{m},k}$, $\hat{R}_t^{350\mu\text{m},k}$ and $\hat{R}_{t_2}^{350\mu\text{m},k} = \hat{Y}_{\max}^{350\mu\text{m},k} - \hat{Y}_{\min}^{350\mu\text{m},k}$ (lines) versus the evaluation length and the means experimental values $Y_{\max}(l)$, $Y_{\min}(l)$ and $R_t(l)$.

It is shown (Karian and Dudewicz, 2000) that $\lambda_3 > -1/4$ and $\lambda_4 > -1/4$ then:

$$\alpha_1 = \lambda_1 + \frac{A}{\lambda_2} \quad (12)$$

$$\alpha_2 = \sigma^2 = \frac{B - A^2}{\lambda_2^2} \quad (13)$$

$$\alpha_3 = \frac{C - 3AB + 2A^3}{\lambda_2^3 \alpha_2^{3/2}} \quad (14)$$

$$\alpha_4 = \frac{D - 4AC + 6A^2B + 3A^4}{\lambda_2^4 \alpha_2^2} \quad (15)$$

with

$$A = \frac{1}{1 + \lambda_3} - \frac{1}{1 + \lambda_4} \quad (16)$$

$$B = \frac{1}{1 + 2\lambda_3} + \frac{1}{1 + 2\lambda_4} - 2\beta(1 + \lambda_3, 1 + \lambda_4) \quad (17)$$

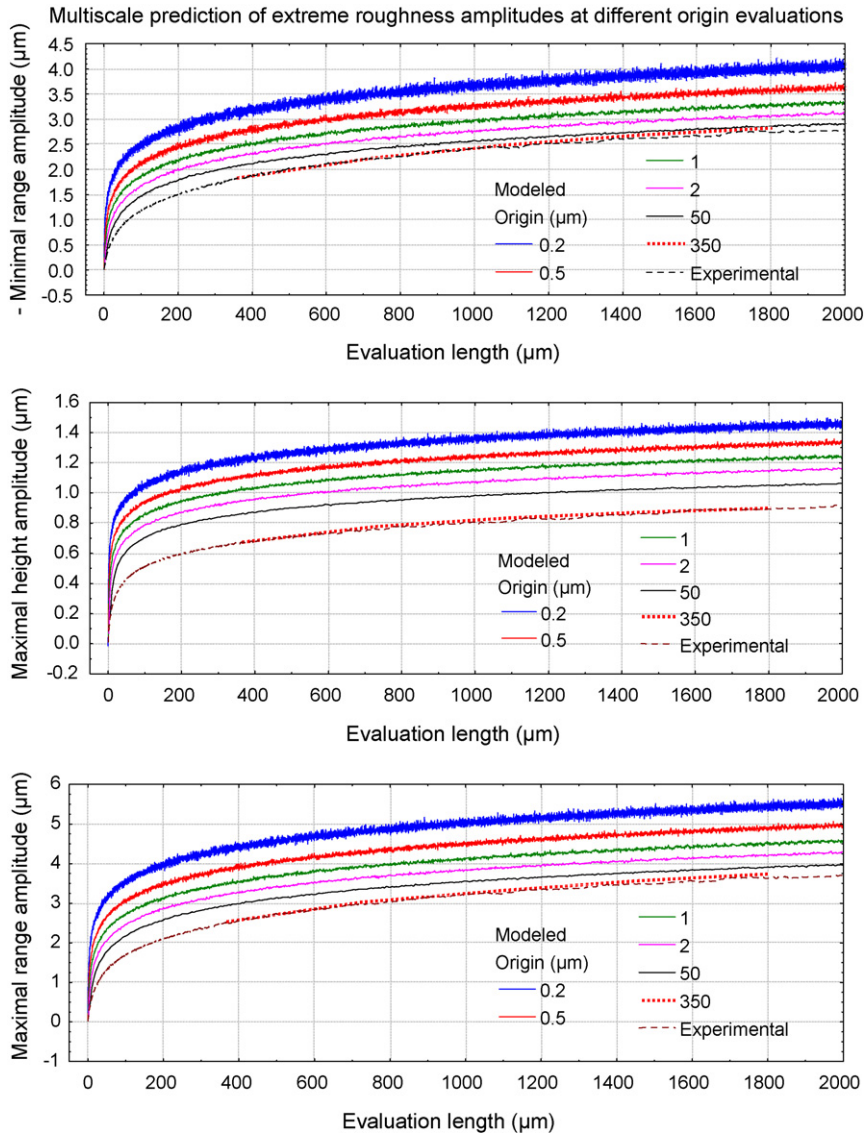


Fig. 18. Multi-scale prediction of extreme roughness amplitudes parameters $\hat{Y}_{\min}^{x,k}$, $\hat{Y}_{\max}^{x,k}$, $\hat{R}_t^{x,k}$ at different origin evaluations $x \in \{0.2, 0.5, 1, 2, 50, 360\}$ and experimental ones (dashed line) $Y_{\max}(l)$, $Y_{\min}(l)$ and $R_t(l)$.

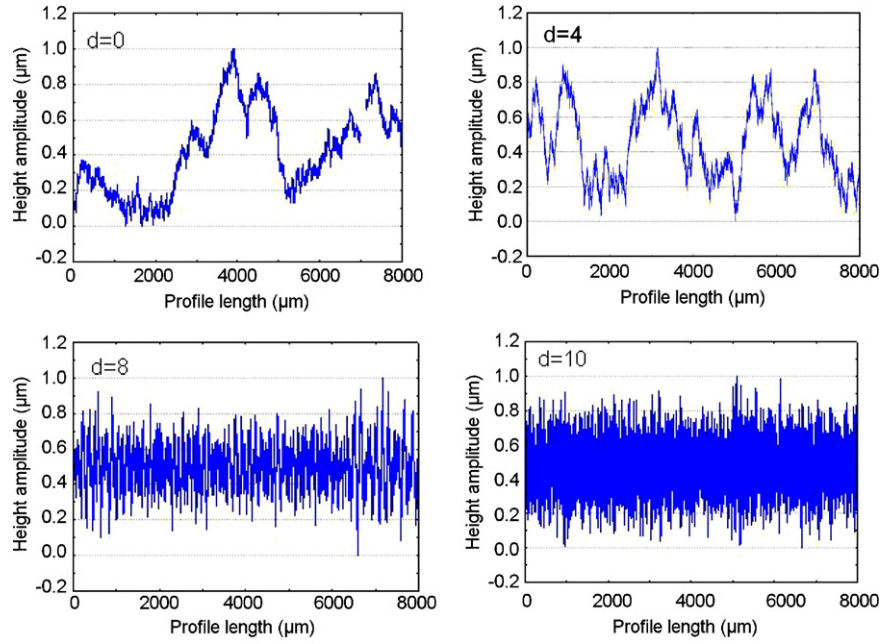


Fig. A.1. Simulated surfaces with modified Weierstrass function obtained with different low frequencies truncation $d=0$ (no truncation), and $d \in \{4, 8, 10\}$.

$$C = \frac{1}{1+3\lambda_3} + \frac{1}{1+3\lambda_4} - 3\beta(1+2\lambda_3, 1+\lambda_4) + 3\beta(1+\lambda_3, 1+2\lambda_4) \quad (18)$$

$$D = \frac{1}{1+4\lambda_3} + \frac{1}{1+4\lambda_4} - 4\beta(1+3\lambda_3, 1+\lambda_4) + 6\beta(1+2\lambda_3, 1+2\lambda_4) - 4\beta(1+\lambda_3, 1+3\lambda_4) \quad (19)$$

where

$$\beta(a, b) = \int_0^1 x^{a-1}(1-x)^{b-1} dx. \quad (20)$$

The moments of $Y_{\max}^x(350 \mu\text{m})$ and $Y_{\min}^x(350 \mu\text{m})$ are reported in Table 2. To calculate $\lambda_1, \lambda_2, \lambda_3$ and λ_4 , α_1 is estimated by $\hat{\alpha}_i$ (Eqs. (8)–(11)) and it is necessary to solve a system of four equations highly non-linear (Eqs. (12), (13), (18) and (19)). As Eqs. (18) and (19) depend only on λ_3 and λ_4 and as $\lambda_2^3 \sigma^3 = (B - A^2)^{3/2}$ and $\lambda_4^4 \sigma^4 = (B - A^2)^2$, the four equations system become a two equations system with more stable numerical convergence (less numerous local extrema). The solutions amounts to find λ_3 and λ_4 by a steepest gradient method on the functional

$$\Psi'(\lambda_3, \lambda_4) = \sum_{i=3}^4 (\hat{\alpha}_i - \alpha_i)^2 \quad (21)$$

and then λ_2 is calculated from Eq. (13) and finally λ_1 from Eq. (12). An algorithm was written and computed using the statistical analyses system language to determine the GLD and its related probability density function from the experimental dataset. The numerical results of the minimization process obtained with our computer algorithm are illustrated in Fig. 15 (left). These figures present a 3D view of the values of the function $\Psi(\lambda_3, \lambda_4)$ on which the optimization algorithm is applied for the lambda distribution associated with $Y_{\max}^x(350 \mu\text{m})$ and $Y_{\min}^x(350 \mu\text{m})$ ($-2 < \lambda_3 < 1$ and $-2 < \lambda_4 < 2$). After minimization, the values of the four parameters for both lambda distributions that modelled $Y_{\max}^x(350 \mu\text{m})$ and $Y_{\min}^x(350 \mu\text{m})$ are obtained (Table 3). Then the $Y_{\max}^x(350 \mu\text{m})$ and $Y_{\min}^x(350 \mu\text{m})$ lambda distribution are plotted in Fig. 15 (right). As it

can be observed, the lambda distributions fit well the $Y_{\max}^x(350 \mu\text{m})$ and $Y_{\min}^x(350 \mu\text{m})$ empirical distributions. To appreciate the accuracy of lambda distribution to model extreme data roughness, a Chi2 criterion is computed. For both data $Y_{\max}^x(350 \mu\text{m})$ and $Y_{\min}^x(350 \mu\text{m})$, the Chi2 criterion does not reject the appropriateness between experimental and model data for usual critical values $\alpha = 0.05$ (respectively $\text{Chi}2_{7df} = 15.99$; $p = 0.07$ and $\text{Chi}2_{7df} = 5.79$; $p = 0.56$). This means that $Y_{\max}^x(350 \mu\text{m})$ and $Y_{\min}^x(350 \mu\text{m})$ both obey a lambda distribution and these models may be used to predict some probabilistic features (Table 3).

5.3. Multi-scale prediction of the maximal, minimal and range amplitude roughness

At this stage, analytical probability density functions (PDF) of $Y_{\max}^x(350 \mu\text{m})$ and $Y_{\min}^x(350 \mu\text{m})$ of the maximal and minimal local roughness amplitude (and thus estimated at the scale $l = 350 \mu\text{m}$) are formulated. Now suppose that the evaluation length is twice the

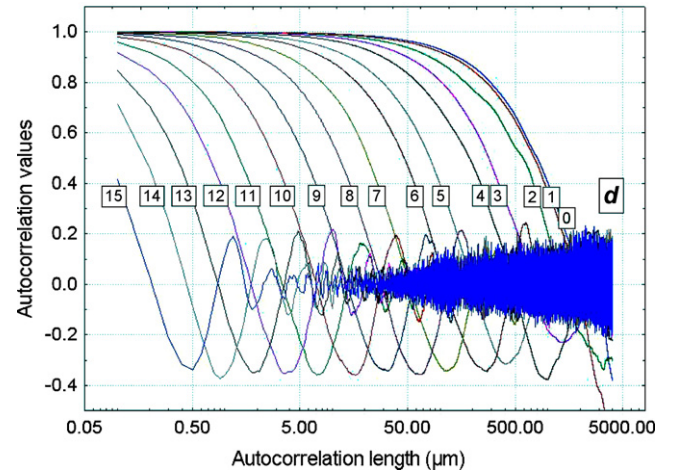


Fig. A.2. Autocorrelation functions of simulated surfaces with modified Weierstrass function obtained with different low frequencies truncation $d=0$ (no truncation), and $d \in \{4, 8, 10\}$ presented in Fig. A.1.

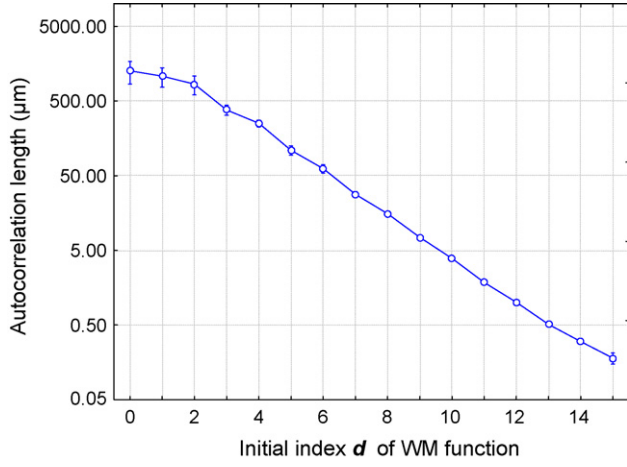


Fig. A.3. Values of autocorrelation lengths of autocorrelation functions presented in Fig. A.2 with their 95% associated confidence intervals.

initial one, i.e. one wants to estimate $Y_{\max}^x(700 \mu\text{m})$. By supposing that at this scale data are independent, then the maximal amplitude $Y_{\max}^{x,x'}(700 \mu\text{m})$ is given by:

$$Y_{\max}^{x,x'}(700 \mu\text{m}) = \max(Y_{\max}^x(350 \mu\text{m}), Y_{\max}^{x'}(350 \mu\text{m})) \quad (22)$$

for two possible values of x and x' .

In an algorithmic point of view, to obtain $Y_{\max}^x(700 \mu\text{m})$, two values that follow $Y_{\max}^x(350 \mu\text{m})$ lambda distribution are generated (using an appropriate random data generator) and a value of $Y_{\max}^x(700 \mu\text{m})$ is then obtained by taking the maximal values of these two generated values. By repeating a high number of times this procedure, the probability density function of $Y_{\max}(700 \mu\text{m})$ can be obtained. This method can be applied at higher scales l : $l = k \times 350 \mu\text{m}$, $k \in \{2, 3, 4, \dots\}$ and the values of $Y_{\max}^x(k \times 350 \mu\text{m})$ are obtained by taking the maximal value from k values generated from the $Y_{\max}^x(350 \mu\text{m})$ lambda distribution. To simulate a random number that follows a lambda distribution of parameters $(\lambda_1, \lambda_2, \lambda_3, \lambda_4)$, the following equation is used:

$$p(u) = \lambda_1 + \frac{(u^{\lambda_3} - (1-u)^{\lambda_4})}{\lambda_2} \quad (23)$$

where u is a uniform random number between 0 and 1 and $p(u)$ is a generated random value.

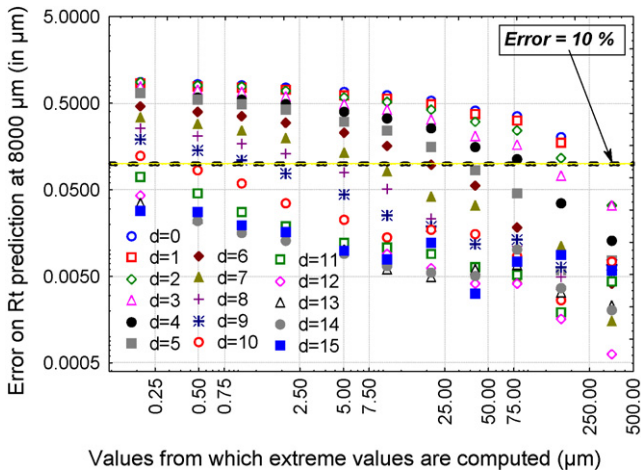


Fig. A.4. Error on R_t prevision at $8000 \mu\text{m}$ versus the windows length (in %) on which extreme values are computed and thus for different d values, i.e. different correlation lengths.

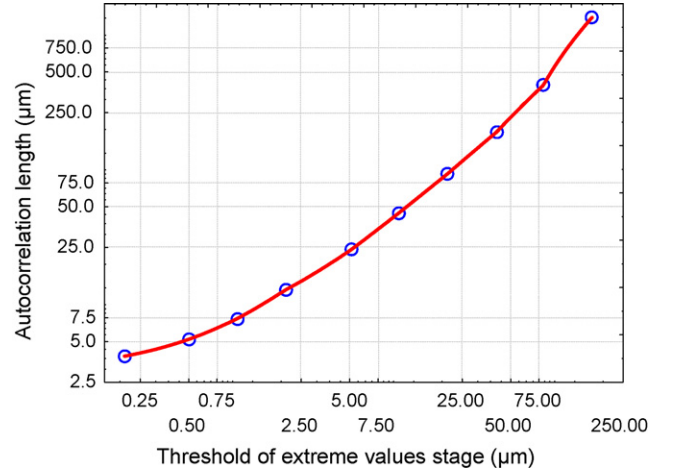


Fig. A.5. Plot of the autocorrelation length versus this critical value (Fig. A.4) representing an error on R_t prevision at $8000 \mu\text{m}$ less than 10%.

In this paper, we note this predicted value $\hat{Y}_{\max}^{l_0,k}$, where l_0 is the length from which extreme roughness is measured and modelled by the lambda distribution, and k is an integer magnification coefficient to predict the extreme roughness amplitude at an evaluation length equal to $l_0 \times k$. To illustrate the prediction method, PDF of $\hat{Y}_{\max}^{350 \mu\text{m},k}$ and $\hat{Y}_{\min}^{350 \mu\text{m},k}$ are computed for $k \in \{1, 2, 5, 10, 20\}$. Fig. 16 represents these PDF functions obtained from 100,000 Monte-Carlo simulations. As it can be observed, the PDF mode increases with magnification k . Fig. 17 represents the means of $\hat{Y}_{\max}^{350 \mu\text{m},k}$, $\hat{Y}_{\min}^{350 \mu\text{m},k}$ and $\hat{R}_t^{350 \mu\text{m},k}$ PDF versus the evaluation length $l = k \times 350 \mu\text{m}$. Without any doubt, it is possible to predict the maximal and minimal roughness at all scales longer than $2000 \mu\text{m}$ by analyzing the roughness at an evaluation length of $350 \mu\text{m}$. However, when the maximal range amplitude $\hat{R}_t^{350 \mu\text{m},k}$ is computed, a high inaccuracy appears in our modelling. The $\hat{R}_t^{350 \mu\text{m},k}$ minimizes the real value to the peak-to-valley parameter amplitude because R_t does not follow an extreme value statistic (Bigerelle et al., 2007). However, to predict its value, it is possible to use the extreme value theory on the minimal and maximal amplitude and thanks to the general relation:

$$\hat{R}_{t2}^{350 \mu\text{m},k} = \hat{Y}_{\max}^{350 \mu\text{m},k} - \hat{Y}_{\min}^{350 \mu\text{m},k} \quad (24)$$

The $\hat{R}_{t2}^{350 \mu\text{m},k}$ parameter models the peaks to valley amplitude from $350 \mu\text{m}$ until more than $1500 \mu\text{m}$ (Fig. 17).

In the preceding case, all previsions of maximal roughness parameters are estimated by taking the origin sampling condition to $l = 350 \mu\text{m}$ (end of the fractal Stage II.a). Now, the same result is proceeded by taking the origin in all the stages (Stages I, II.a, II.b) ($l_0 \in \{0.2, 0.5, 1, 2, 50, 360\} \mu\text{m}$). Fig. 18 shows the evolution of the three predicted roughness parameters $\hat{R}_{t2}^{l_0,k}$, $\hat{Y}_{\max}^{l_0,k}$ and $\hat{Y}_{\min}^{l_0,k}$ for these different origins l_0 . As it is observed for all parameters, the predictions always hold for $l = 350 \mu\text{m}$, i.e. greater than the autocorrelation length, with a very good accuracy. This means that the sub-stage II.b described in our section is an extreme value stage and that the other stages do not exhibit this structure as we have claimed in the preceding chapters. Some more cases are tested to check our results: simulations are then carried out on a Weierstrass function that we have modified to obtain different autocorrelation lengths with same fractal dimension (Appendix A). To limit the R_t prediction error at less than 10%, the threshold value l_0 must be higher than half the autocorrelation length.

6. Conclusion

The multi-scale analysis shows that belt finishing process creates a fractal structure on tooled surfaces until a critical length that is related to the profile autocorrelation length. When surfaces are recorded by a tactile profilometer, a stage that represents a smoothing effect due to the tip of curvature and less or equal to the tip radius diameter appears. It has been shown that the fractal stage does not present a linear part (in a log-log plot) due to a bias in sampling. If a fixed number of data is used to compute roughness parameters in the multi-scale windows, then a perfect linear relation emerges and allows to perfectly calculate the fractal dimension. We also show that experimental surfaces obtained by BFP can be modelled by fractal functions and a stochastic model at all scales. After the fractal threshold, a stage is characterized by the extreme values theory. An alternative methodology to the Gumbel approach was presented in order to estimate accurately the maximal peaks and minimal valleys. Based on the generalized lambda distribution and the Monte-Carlo simulation, the distribution of extreme values is predicted on a range greater than the measured one with confidence interval of the maximal valleys and peaks and also the roughness parameters "peak-to-valley". This methodology is a contribution to estimate control tolerance in the field of high precision surfaces obtained by abrasion processes and may be applied to other tooled surfaces.

Acknowledgment

This work was supported by the CETIM (Centre Technique des Industries Mécaniques) foundation, located at Senlis (France) in the Project "Nouvelles méthodes d'analyse des états de surfaces: de la caractérisation à la recherche de paramètres pertinents".

Appendix A. Determination of the threshold of the extreme values stage

We have shown that the extreme values stage holds if the threshold from which the extreme values are predicted is greater than the autocorrelation length. To verify this purpose, the Weierstrass fractal function is used and extreme value stage is computed. The Weierstrass function is defined as follows:

$$w(x) = \sum_{n=0}^{n=+\infty} a_n w^{-nH} (\cos(w^n x + \varphi_n))$$

where $\Delta = 2 - H$ is the fractal dimension, a_n gaussian random numbers and φ_n uniform random numbers belonging to the range 0 and 2π .

We modify this function as follows:

$$w(x) = A \sum_{n=d}^{n=+\infty} a_n w^{-nH} (\cos(w^n x + \varphi_n))$$

This transformation does not change the fractal dimension but the function has lost its statistical self-affinity. This function is normalized to unity in amplitude with the A factor. As a consequence, the higher d is, the lower the low frequencies amplitude is then the lower the autocorrelation length is. We have selected the value for the fractal dimension $\Delta = 1.5$ (Brownian motion). 10 profiles are simulated for each d value, d varying from 0 to 15. (Fig. A.1). Fig. A.2 represents the mean autocorrelation functions. As it can be observed, the autocorrelation length decreases logarithmically with respect to the d value (Fig. A.3). Then the extreme values are computed from a given origin and the error on R_t at $8000 \mu\text{m}$ is evaluated. Fig. A.4 represents the error on R_t prevision at $8000 \mu\text{m}$ versus the windows length (in %) on which extreme values are

computed and thus for different d values, i.e. different correlation lengths. For a given d , error on R_t predicted at $8000 \mu\text{m}$ decreases with the values from which extreme values are computed. For a given initial values from which extreme values are computed, the error decreases with d value, i.e. the autocorrelation length decreases. An error less than 10% is fixed on the R_t prediction and the minimal values from which extreme values must be computed to guaranty this prediction is evaluated. Finally, the autocorrelation length is plotted versus this critical value (Fig. A.5) that shows that the windows from which the extreme value stage holds lies around 50% of the autocorrelation length of the profile.

References

- Axinte, D.A., Kritmanorot, M., Axinte, M., Gindy, N.N.Z., 2005. Investigations on belt polishing of heat-resistant titanium alloys. *J. Mater. Process. Technol.* 166 (3), 398–404.
- Axinte, D.A., Kwong, J., Kong, M.C., 2009. Workpiece surface integrity of Ti-6-4 heat-resistant alloy when employing different polishing methods. *J. Mater. Process. Technol.* 209 (4), 1843–1852.
- Belkhir, N., Bouzid, D., Herold, V., 2007. Correlation between the surface quality and the abrasive grains wear in optical glass lapping. *Tribol. Int.* 40 (3), 498–502.
- Bhushan, B., Majumdar, A., 1992. Elastic-plastic contact model for bifractal surfaces. *Wear* 153 (1), 53–64.
- Bigerelle, M., Gautier, A., Iost, A., 2007. Roughness characteristic length scales of micro-machined surfaces: a multi-scale modeling. *Sens. Actuators, B* 126 (1), 126–137.
- Bigerelle, M., Iost, A., 1999. Bootstrap analysis of fatigue crack growth rate: application on the Paris' relationship and to lifetime prediction. *Int. J. Fatigue* 21 (4), 299–307.
- Bigerelle, M., Najjar, D., Iost, A., 2005. Multiscale functional analysis of wear: a fractal model of the grinding process. *Wear* 258 (1–4), 232–239.
- Bigerelle, M., Hagege, B., El Mansori, M., 2008. Mechanical modelling of micro-scale abrasion in superfinish belt grinding. *Trib. Int.* 41 (11), 992–1001.
- Brinksmeier, E., Riemer, O., Gessenharter, A., 2006. Finishing of structured surfaces by abrasive polishing. *Precision Eng.* 30 (3), 325–336.
- Campbell, J.H., Hawley-Fedder, R.A., Stolz, C.J., Menapace, J.A., Borden, M.R., Whitman, P.K., Yu, J., Runkel, M., Riley, M.O., Feit, M.D., Hackel, R.P., 2004. NIF optical materials and fabrication technologies: an overview. *Proc. SPIE* 5341, 84–101.
- Chang, L., 1995. Deterministic modeling and numerical simulation of lubrication between rough surfaces—a review of recent developments. *Wear* 184, 155–160.
- Chang, S.H., Farris, T.N., Chandrasekarc, S., 2008. *J. Mater. Process. Technol.* 203, 365–371.
- Cheng, H.S., 2002. Analytical modeling of mixed lubrication performance. In: *Boundary and Mixed Lubrication: Science and Applications, Proceedings of the 28th Leeds-Lyon Symposium on Tribology*. Elsevier, Amsterdam, pp. 19–33.
- Cho, S.S., Ryu, Y.K., Lee, S.Y., 2002. Curved surface finishing with flexible abrasive tool. *Int. J. Mach. Tools Manufact.* 42, 229–236.
- Dalla Costa, M., Bigerelle, M., Najjar, D., 2007. A new methodology for quantifying the multi-scale similarity of images. *Microelectron. Eng.* 84 (3), 424–430.
- Das, M., Jain, V.K., Ghoshdastidar, P.S., 2008. Fluid flow analysis of magnetorheological abrasive flow finishing (MRAFF) process. *Int. J. Mach. Tools Manufact.* 48 (3–4), 415–426.
- Dubuc, B., Quiniou, J.F., Roques-Carnes, C., Tricot, C., Zucker, S.W., 1989. Evaluating the fractal dimension of profiles. *Phys. Rev. A* 393, 1500–1512.
- El-Axira, M.H., Othmanb, O.M., Abodienac, A.M., 2008. Study on the inner surface finishing of aluminum alloy 2014 by ball burnishing process. *J. Mater. Process. Technol.* 202, 435–442.
- Fine, K.R., Garbe, R., Gip, T., Nguyen, Q., 2005. Non-destructive, real time direct measurement of subsurface damage. *Proc. SPIE* 5799, 105–110.
- Giljean, S., Bigerelle, M., Anselme, K., 2007. A multiscale topography analysis of ground stainless steel and titanium alloys. *Revue Proceedings of the Institution of Mechanical Engineers, Part B: Journal of Engineering Manufacture* 221. (9).
- Giljean, S., Najjar, D., Bigerelle, M., Iost, A., 2008. Multiscale analysis of abrasion damage on stainless steel. *Surf. Eng.* 24 (1), 8–17.
- Grzesik, W., Rech, J., Wanat, T., 2007. Surface finish on hardened bearing steel parts produced by superhard and abrasive tools. *Int. J. Mach. Tools Manufact.* 47 (2), 255–262.
- Gumbel, E.J., 1954. *Statistical Theory of Extreme Values and Some Practical Applications*. In: *Appl. Maths.* (33). National Bureau of Standards, Washington, D.C.
- Hasegawa, M., Liu, J., Okuda, K., 1996. Calculation of the fractal dimension of machined surface profiles. *Wear* 192, 40–45.
- He, L., Zhu, J., 1997. The fractal character of processed metal surfaces. *Wear* 208 (1–2), 17–24.
- Hed, P.P., Edwards, D.F., 1987. Optical glass fabrication technology. 2. Relationship between surface roughness and subsurface damage. *Appl. Opt.* 26 (21), 4677–4680.
- Jain, R.K., Jain, V.K., Dixit, P.M., 1999. Modeling of material removal and surface roughness in abrasive flow machining process. *Int. J. Mach. Tools Manufact.* 39, 1903–1923.
- Jha, S., Jain, V.K., 2006. Modeling and simulation of surface roughness in magnetorheological abrasive flow finishing (MRAFF) process. *Wear* 261, 856–866.

- Journal, A., Dursapt, M., Hamdi, H., Rech, J., Zahouani, H., 2005. Effect of the belt grinding on the surface texture: modeling of the contact and abrasive. *Wear* 259, 1137–1143.
- Karian, Z.A., Dudewicz, E.J., 2000. *Fitting Statistical Distributions, The Generalized Lambda Distribution and Generalized Bootstrap Methods*. Chapman & Hall, CRC Press, Boca Raton, FL.
- Khellouki, A., Rech, J., Zahouani, H., 2007. The effect of abrasive grain's wear and contact conditions on surface texture in belt finishing. *Wear* 263 (1–6), 81–87.
- Krupka, I., Koutny, D., Hartl, M., 2008. Behavior of real roughness features within mixed lubricated non-conformal contacts. *Tribol. Int.* 41, 1153–1160.
- Lopez, J., Hansali, G., Le Bossa, J.C., Mathia, T., 1994. Caractérisation fractale de la rugosité tridimensionnelle d'une surface. *J. Phys. III* 4, 2501–2519.
- Li, S., Wang, Z., Wu, Y., 2008. Relationship between subsurface damage and surface roughness of optical materials in grinding and lapping processes. *J. Mater. Process. Technol.* 205, 34–41.
- Mandelbrot, B.B., 1983. *The Fractal Geometry of Nature*. W.H. Freeman & Company, New York.
- Mandelbrot, B.B., Van Ness, J.W., 1968. Fractional Brownian motions, fractional noises and applications. *SIAM Rev.* 10, 422–437.
- Mazeran, P.-E., Odoni, L., Loubet, J.-L., 2005. Curvature radius analysis for scanning probe microscopy. *Surf. Sci.* 585 (1–2), 25–37.
- Mc Cool, J.I., 1986. Comparison of models for the contact of rough surfaces. *Wear* 107, 37–60.
- Mezghani, S., El Mansori, M., Zahouani, H., 2009. New criterion of grain size choice for optimal surface texture and tolerance in belt finishing production. *Wear* 266 (5–6), 578–580.
- Miller, P.E., Suratwala, T.I., Wong, L.L., Feit, M.D., Menapace, J.A., Davis, P.J., Steele, R.A., 2005. The distribution of subsurface damage in fused silica. *Proc. SPIE* 5991, 1–25.
- Najjar, D., Bigerelle, M., Iost, A., 2003. The computer-based bootstrap method as a tool to select a relevant surface roughness parameter. *Wear* 254 (5–6), 450–460.
- Novovic, D., Dewes, R.C., Aspinwall, D., Voice, K.W., Bowen, P., 2004. The effect of machined topography and integrity on fatigue life. *Int. J. Mach. Tools Manufact.* 44, 125–134.
- Nakamura, T., 1966. On deformation of surface roughness curves caused by finite radius of stylus tip and tilting of stylus holder arm. *Bull. Jpn. Soc. Precision Eng.* 1, 240–248.
- Ohlsson, R., Wihlborg, A., Westberg, H., 2001. The accuracy of fast 3D topography measurements. *Int. J. Mach. Tools Manufact.* 41 (13–14), 1899–1907.
- Puthanangady, T.K., Malkin, S., 1995. Experimental investigation of the superfinishing process. *Wear* 185, 173–182.
- Poon, C.Y., Bhusham, B., 1995. Comparison of surface roughness measurements by stylus profiler, AFM, and non-contact optical profiler. *Wear* 190, 76–88.
- Radhakrishnan, V., 1970. Effect of stylus radius on the roughness values measured with tracing stylus instruments. *Wear* 16, 325–335.
- Ramos, A.M., Relvas, C., Simões, J.A., 2003. The influence of finishing milling strategies on texture, roughness and dimensional deviations on the machining of complex surfaces. *J. Mater. Process. Technol.* 136 (1–3), 209–216.
- Randi, J.A., Lambropoulos, J.C., Jacobs, S.D., 2005. Subsurface damage in some single crystalline optical materials. *Appl. Opt.* 44 (12), 2241–2249.
- Retherford, R.S., Sabia, R., Sokira, V.P., 2001. Effect of surface quality on transmission performance for (1 1 1) CaF₂. *Appl. Surf. Sci.* 183, 264–269.
- Rech, J., Kermouche, G., Grzesik, W., García-Rosales, C., Khellouki, A., García-Navas, V., 2008. Characterization and modelling of the residual stresses induced by belt finishing on a AISI52100 hardened steel. *J. Mater. Process. Technol.* 208 (1–3), 187–195.
- Ryua, S.H., Choib, D.K., Chuc, C.N., 2006. Roughness and texture generation on end milled surfaces. *Int. J. Mach. Tools Manufact.* 46, 404–412.
- Shen, J., Liu, S., Yi, K., He, H., Shao, J., Fan, Z., 2005. Subsurface damage in optical substrates. *Optik* 116, 288–294.
- Sheiko, S.S., Möller, M., Reuvekamp, E.M.C.M., Zandbergen, H.W., 1994. Evaluation of the probing profile of scanning force microscopy tips. *Ultramicroscopy* 53 (4), 371–380.
- Singh, K., Jain, V.K., Raghurama, V., Komanduri, R., 2005. Analysis of surface texture generated by a flexible magnetic abrasive brush. *Wear* 259, 1254–1261.
- Spikes, H.A., Olver, A.V., 2002. Basics of mixed lubrication. In: *Lubricants, Materials, and Lubrication Engineering. Proceedings of 13th International Colloquium Tribology*. Ostfildern, Technische Akademie Esslingen, pp. 2037–2040.
- Spitzer, 1976. *Principles of Random Walks*. Graduate Texts in Mathematics, vol. 34. Springer-Verlag, New York, Heidelberg.
- Stephenson, D.J., Veselovac, D., Manley, S., Corbett, J., 2001. Ultra-precision grinding of hard steels. *Precision Eng.* 25 (4), 336–345.
- Stolz, C.J., Menapace, J.A., Schaffers, K.I., Bibeau, C., Thomas, M.D., Griffin, A.J., 2005. Laser damage initiation and growth of antireflection coated S-FAP crystal surfaces prepared by pitch lap and magnetorheological finishing. *Proc. SPIE* 5991, 449–455.
- Suzuki, H., Moriwaki, T., Okino, T., Ando, Y., 2006. Development of ultrasonic vibration assisted polishing machine for micro aspheric die and mold. *CIRP Ann. – Manuf. Technol.* 55 (1), 385–388.
- Takaya, Y., Hida, K., Miyoshi, T., Hayashi, T., 2006. A novel surface finishing technique for microparts using an optically controlled microparticle tool. *CIRP Ann. – Manuf. Technol.* 55 (1), 613–616.
- Thomas, T.R., Rosén, B.G., Amini, N., 1999. Fractal characterisation of the anisotropy of rough surfaces. *Wear* 232 (1), 41–50.
- Tricot, C., 1993. *Courbes et Dimension Fractale*. Springer-Verlag, Paris.
- Varghese, B., Malkin, S., 1995. Experimental investigation of methods to enhance stock removal for superfinishing. *Ann. CIRP* 47 (1), 231–234.
- Wang, Y., Hu, D., 2005. Study on the inner surface finishing of tubing by magnetic abrasive finishing. *Int. J. Mach. Tools Manuf.* 45 (1), 43–49.
- Wani, Amit, M., Yadava, V., Khatri, A., 2007. Simulation for the prediction of surface roughness in magnetic abrasive flow finishing (MAFF). *J. Mater. Process. Technol.* 190, 282–290.
- Whebi, D., 1986. *Approche fractale de la rugosité des surfaces et implication analytique*. PhD Thesis, Besançon, France.
- Whitehouse, D.J., 1974. Theoretical analysis of stylus integration. *Ann. CIRP* 23, 181–182.
- Whitehouse, D.J., 1994. *Handbook of Surface Metrology*. Institute of Physics Publishing, Bristol.
- Wu, J.J., 2000. Characterization of fractal surfaces. *Wear* 239 (1), 36–47.
- Wu, J.J., 2001. Structure function and spectral density of fractal profiles. *Chaos. Solitons & Fractals* 12 (13), 2481–2492.
- Yamaguchi, H., Shinmura, T., 1999. Study of the surface modification resulting from an internal magnetic abrasive finishing process. *Wear* 225–229 (1), 246–255.
- Zhanga, L., Tsunemoto, K., Tsuyoshi, K., Ji, Z., 2005. Investigation into electrorheological fluid-assisted polishing. *Int. J. Mach. Tools Manuf.* 45, 1461–1467.
- Zhou, G., Lam, N.S., 2005. A comparison of fractal dimension estimators based on multiple surface generation methods. *Comput. Geosci.* 31 (10), 1260–1269.